Correlation between Zn vacancies and photoluminescence emission in ZnO films

A. Zubiaga[a] and J. A. García
Fisika Aplikatua II Saila, Euskal Herriko Unibertsitatea, Posta Kutxatila 644, 48080 Bilbao, Spain

F. Plazaola, F. Tuomisto, and K. Saarinen
Laboratory of Physics, Helsinki University of Technology, 02150 Espoo, Finland

J. Zuñiga Pérez and V. Muñoz-Sanjosé
Universitat de València, Departamento de Fisíca Aplicada i Electromagnetisme, c/Doctor Moliner 50, E-46100 Burjassot, València, Spain

(Received 28 July 2005; accepted 17 January 2006; published online 9 March 2006)

Photoluminescence and positron annihilation spectroscopy have been used to characterize and identify vacancy-type defects produced in ZnO films grown on sapphire by metal-organic chemical-vapor deposition. The photoluminescence of the samples in the near band edge region has been studied, paying particular attention to the emission at 370.5 nm (3.346 eV). This emission has been correlated to the concentration of Zn vacancies in the films, which has been determined by positron annihilation spectroscopy. © *2006 American Institute of Physics*.
[DOI: 10.1063/1.2175476]

I. INTRODUCTION

The physical and chemical properties of ZnO and the progress in crystal growth processes[1] have renewed the interest on this material due to the potentials it presents in different technological fields, particularly in optoelectronic devices working at blue and ultraviolet wavelengths. In fact, ultraviolet laser emission at room temperature has been reported for ZnO thin films.[2,3] On the other hand, due to the relative low cost of sapphire substrates, its availability in large area wafers and its transparency up to about 6 μm light wavelength, sapphire is a potential substrate for mass production of ZnO films and it has been largely used for investigating that material. However, the heteroepitaxy of ZnO on sapphire presents several problems due to differences in their chemical nature, structure (wurtzite or corundum), and lattice parameters.[4] For instance, Srikant and Clarke[5] showed that the optical absorption coefficient and the band edge characteristic of the ZnO films are not only sensitively dependent on the microstructure of the films but on the nature of the substrates too. A necessary step, prior to the technological and practical use of ZnO in optoelectronics, is the knowledge of the ZnO/sapphire interface microstructure in order to control the defects of the deposited films and to improve the quality of the final devices.

Defects in ZnO are characterized by different experimental methods, photoluminescence (PL) being one of the most relevant. The excitonic emission lines of ZnO thin films have been widely discussed but the interest in this subject continues with the aim of clarifying the physical origin of the emissions. On the other hand, positron annihilation spectroscopy has been shown to be a promising technique for studying the defect structure in ZnO films.[6,7] In this article we apply PL and positron annihilation spectroscopy for characterizing some open volume defects, to which these techniques are sensitive, created in the growth by metal-organic chemical-vapor deposition (MOCVD) of ZnO layers on sapphire substrates with different orientations.

II. EXPERIMENT

ZnO films were grown by MOCVD on sapphire substrates of two different orientations (0001) and (1-102), which in the following we will refer to as *C* and *R* planes, respectively. Two strategies for the growth were used: a direct growth on the sapphire substrates and a growth on a ZnO buffer layer, grown at 350 °C for 4 min (the estimated buffer layer thickness is about 60–70 nm).

In both cases the growth temperature was 420 °C using DMZn-TMA and tert-butanol as zinc and oxygen precursors and nitrogen as carrier gas. The deposition time was 7200 s in all the cases and the final thickness was in the order of 2000 nm. A detailed discussion about the surface morphology and MOCVD growth conditions of the samples studied in this work is presented in Ref. 8.

Temperature dependent PL measurements were performed using the laser port of a CD900 spectrometer system from Edinburgh Instruments, with an R955 photomultiplier in a Peltier cooled housing. Samples were excited by means of the 325 nm line of a 50 mW He–Cd laser and measurements were performed between 10 and 300 K using a closed cycle helium cryostat. All spectra were taken under the same conditions, that is, same excitation power, sample orientation with respect to the laser beam, monochromator slit apertures, and all the other control parameters.

The positron experiments were performed at room temperature with a monoenergetic positron beam. The energy of the beam was varied in the 0–40 keV range and the Doppler broadening of the annihilation radiation was measured for all positron implantation energies. Positrons get trapped at

[a]Electronic mail: asier.zubiaga@ehu.es

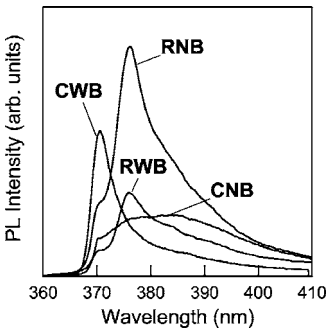

FIG. 1. Photoluminescence emission at 10 K, excited at 325 nm for sample CWB, grown over the *C* plane of sapphire with buffer; sample CNB, grown over the *C* plane of sapphire without buffer; sample RWB, grown over the *R* plane of sapphire with buffer; and sample RNB, grown over the *R* plane of sapphire without buffer.

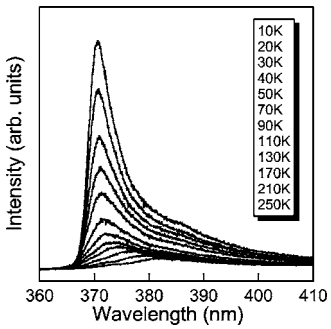

FIG. 2. Emission spectra of the 370.5 nm (3.346 eV) emission of CWB sample in Fig. 1 for different temperatures. All spectra have the same scale and are presented from 10 to 250 K in intensity decreasing order, respectively.

vacancy-type defects, and their annihilation characteristic changes with respect to the annihilation from the delocalized state. The Doppler broadening of the annihilation radiation gives information about the electron momentum distribution at the annihilation site. The Doppler broadening of the annihilation radiation was measured using a Ge detector with an energy resolution of 1.24 keV at 511 keV. To characterize the spectra, the used energy windows were $|E_\gamma\text{-}511\ \text{keV}| \leqslant 0.8\ \text{keV}$ $(p_L/m_0c \leqslant 3\times10^{-3}$, where m_0 is the electron mass) for the central S parameter and $2.9\ \text{keV} < |E_\gamma\text{-}511\ \text{keV}| \leqslant 7.4\ \text{keV}$ $(11\times10^{-3} \leqslant p_L/m_0c \leqslant 29\times10^{-3})$ for the wing W parameter.[9] An as-grown ZnO bulk sample that does not present traps for positrons at room temperature and has a positron lifetime of 170 ps (Ref. 10) was used as a reference sample.

III. RESULTS AND DISCUSSION

Figure 1 shows the results for the PL emission in the near band edge region, at 10 K, corresponding to four different samples. The RWB and RNB samples (for sample's nomenclature, see Table I) present a dominant excitonic peak at 375.5 nm (3.302 eV), while the CNB sample shows a wider emission which has two main components, the above mentioned at 375.5 nm and other at around 384 nm. In addition, the three samples present a lower intensity high energy component at 370.5 nm (3.346 eV). However, the CWB sample has a very different PL emission, in this case, the PL shows a peak at 370.5 nm (3.346 eV) as the main feature. This fact points to a different concentration of the center related to this emission as compared with the other samples. In the following we will focus on this emission that seems to be present in all the cases but with a different related-center concentration.

TABLE I. Concentration of Zn vacancies ($C_{V_{Zn}}$) in ZnO films grown over *C* and *R* planes of sapphire. In the films with buffer layer, the buffer was grown for 4 min at 350 °C.

Sample's nomenclature	Estimated thickness (μm)	Growth plane	Buffer layer	$C_{V_{Zn}}$ (ppm)
RWB	2	*R*	Yes	1.7(3)
RNB	2	*R*	No	1.7(3)
CWB	2	*C*	Yes	6(2)
CNB	2	*C*	No	1.9(3)
M	0.5	*M*	No	2.0(3)
A	0.5	*A*	No	3.7(8)
C	0.5	*C*	No	7(2)

Figure 2 shows the temperature dependence of the 370.5 nm emission for the CWB sample. The activation energy for this recombination can be determined from the luminescence quenching. Figure 3 shows the integrated PL intensity of the 370.5 nm recombination as a function of the inverse temperature. Taking into account that the PL measurements are performed in continuous mode and at different temperatures, the experimental results can be well fitted considering a one-step quenching process[11] described by

$$I_{\text{PL}} = \frac{I_0}{1 + C\exp(-E_{\text{act}}/K_BT)}, \tag{1}$$

in which the activation energy acts as a fitting parameter that can be obtained from the experimental curve. This fit gives a value for the activation energy of $E_{\text{act}}=9.3\pm0.1$ meV, being of the same order as the one corresponding to a bound exciton recombination.[12,13]

Figure 4 shows the temperature dependence of the peak's position corresponding to the 370.5 nm (3.346 eV) emission. Due to the excitonic character of this recombination, we can use the Varshni's equation[14] to fit the temperature dependence:

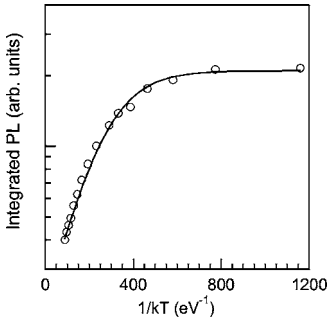

FIG. 3. Photoluminescence intensity quenching of the 370.5 nm (3.346 eV) emission of CWB sample as a function of $(1/kT)$. The fitted function is presented too.

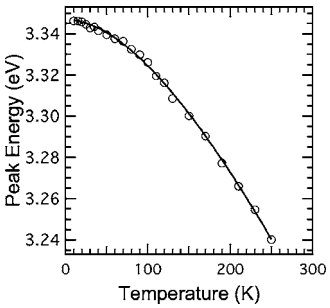

FIG. 4. Peak position of the 370.5 nm (3.346 eV) emission, corresponding to the CWB sample, as a function of temperature, fitted with the Varshni semiempirical function.

$$E(T) = E(0) - \alpha \frac{T^2}{T+\beta}, \tag{2}$$

where α and β are constants and, in the measured range of temperatures, we can take β to be equal to the Debye temperature Θ_D.[15] The fitting of the experimental values presented in Fig. 4 gives the following values for the parameters: $\alpha=(1.1\pm0.09)\times10^{-3}$ eV/K and $\beta=377\pm51$ K. In the literature, different values for the Debye temperature are found. Kaldis[16] gives a value for $\Theta_D=416$ K while other authors[17,18] reported values of 370 and 516 K, respectively. The obtained value of 377 K, in our work, is in reasonable agreement with those values, corroborating the excitonic character of the emission.

In order to estimate the ionization energy of the center responsible for the 370.5 nm (3.346 eV) emission we have used the relation proposed by Haynes[19] between the ionization energy of the associated center E_I and the localization energy of the excitonic emission peak $E_{\mathrm{loc}}=a+b\times E_I$.

The localization energy is $E_{\mathrm{loc}}=E_{\mathrm{FX}}-E_{\mathrm{BX}}$, where E_{FX} is the free exciton energy and E_{BX} is the energy of the bound exciton. Assuming a value of 3.376 eV for E_{FX} and using the values $a=-3.8$ meV and $b=0.365$, obtained by Meyer *et al.*[13] from the excitonic lines I_4-I_{10} in bulk ZnO, the ionization energy can be determined to be 93 meV. Different values, $a=-0.021$ meV and $b=0.244$ which were obtained by Gutowski *et al.*[20] by analyzing the I_5-I_{11} lines, can also be used. In this case the calculated ionization energy would be 123 meV.

The above results and the classification of the PL lines in ZnO proposed by Studenikin *et al.*[21] allow us to assign the 370.5 nm emission to the recombination of an exciton in a deep center. In addition, due to the proximity of this peak to the reported I_{11} emission line (3.348 eV) of excitons bound at neutral acceptors,[20] we can suggest that the 370.5 nm (3.346 eV) line is due to the recombination of excitons into deep acceptor centers.

In order to identify the acceptor defect responsible for this 370.5 nm recombination we have performed positron annihilation spectroscopy. Figure 5 shows the *S* and *W* parameters obtained for the ZnO reference sample (full squares and full circles) when varying the energy of the implanted positrons. The *W*/*S* plot shows a straight line, which is presented in Fig. 7 (full circles), in which the upper left corner corresponds to the *S* and *W* parameters of the ZnO lattice ($S=1$ and $W=1$). The straight line indicates that there are only two states where positrons annihilate. At very low implantation energies the positrons are preferentially annihilating from surface states (bottom right corner in the figure) but at high implantation energies almost all the positrons annihilate from the delocalized state in the bulk of the material.

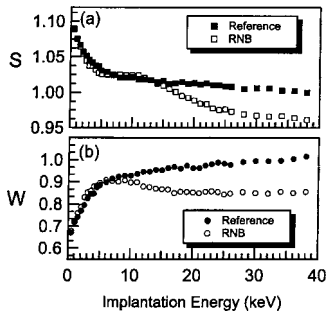

FIG. 5. ZnO reference sample and ZnO film grown over *R* plane sapphire without buffer layer (RNB sample). (a) *S* parameter vs energy of the implanted positrons (reference sample full square, RNB sample empty square) and (b) *W* parameter vs energy of the implanted positrons (reference sample full circle, RNB sample empty circle).

The *S* and *W* parameters measured in the ZnO films grown over *C* and *R* sapphire substrates, with and without buffer layer, show a completely different behavior as compared to the reference sample. For comparison, Fig. 5 also shows the *W* and *S* parameters corresponding to the RNB sample (empty squares and empty circles) as representative for the positron annhilation behavior of all the studied samples. In Fig. 6, the other used samples grown over *C* and *R* sapphire substrates, with and without buffer layer, are compared. At low implantation energies, the *W* and *S* parameters are very close to the values of the reference sample, indicating similar surface positron states. At higher implantation energies the *W*/*S* curve follows a straight line towards a cusp, the (*S*, *W*) position of which depends on the measured film. This is a clear indication that positrons are annihilating at surface states and bulk states inside the film. At implantation energies higher than the one corresponding to the cusp, the measured values do not follow the previous straight line and they tend toward a new position that is quite the same in all the studied films (see Fig. 7 for the RNB sample and Fig. 8 for all the other measured samples). The position, obtained at high implantation energies, corresponds

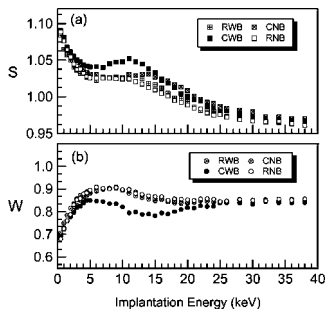

FIG. 6. *S* parameters (a) and *W* parameters (b) vs energy of the implanted positrons of ZnO films grown over *R* sapphire without buffer (RNB), *R* sapphire with buffer (RWB), *C* sapphire without buffer (CNB), and *C* sapphire with buffer (CWB). Same scale as in Fig. 5 is used.

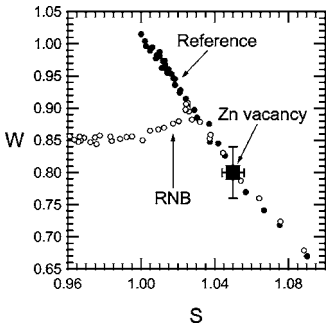

FIG. 7. *W*/*S* plot corresponding to the reference (full circle) and RNB (empty circle) samples in Fig. 5.

to positron annihilation at the bulk of the sapphire. It is interesting to notice that the sapphire parameters are very similar in all the measured samples. Following the previous reasoning and taking into account the results of Ref. 9, we can assume that the highest positron annihilation probability at the bulk of ZnO films corresponds to the cusp of the *W*/*S* plot.

Figure 9 shows the *W*/*S* plot of the above cited cusp positions obtained for the ZnO films grown over *C* and *R* planes with and without buffer layer, together with the cusp positions obtained for ZnO thinner films grown without buffer layer (see Ref. 9) on *M*(10-10), *A*(11-20), and *C*(0001) planes of sapphire. In the figure, the *W* and *S* parameters for the bulk reference sample and the saturated trapping at Zn vacancies are shown too. *W* and *S* parameters of the bulk reference sample correspond to annihilation from delocalized states. *W* and *S* parameters corresponding to saturation trapping at Zn vacancies have been estimated from simultaneous lifetime and Doppler measurements in bulk ZnO samples.[10] The measured values fall within a straight line in the *W*/*S* plot presented in Ref. 9 indicating that the defect trapping positrons are the same in all the studied ZnO films independent of (i) the sapphire plane over which were grown, (ii) the presence of a buffer layer, and (iii) the thickness, i.e., the Zn vacancy.

Taking into account the kinetic trapping model[22] the fraction of positrons annihilating at Zn vacancies (η_D) and the positron trapping rate (K_D) into them are written as

$$\eta_D = \frac{S - S_B}{S_D - S_B} = \frac{W - W_B}{W_D - W_B}, \tag{3}$$

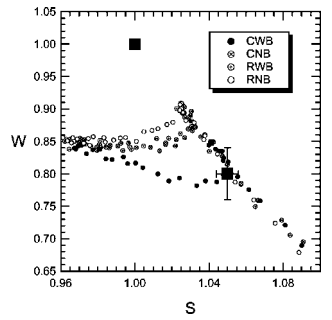

FIG. 8. *W*/*S* plot corresponding to the samples shown in Fig. 6.

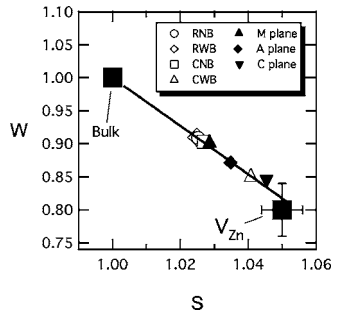

FIG. 9. *W*/*S* plot of the cusp positions corresponding to ZnO films in Fig. 1. Cusp position for other three samples grown over *M*, *A*, and *C* planes is also indicated in full symbols.

$$K_D = \frac{\eta_D \lambda_B}{1 - \eta_D}, \tag{4}$$

where the subscripts *B* and *D* indicate positrons at delocalized state and positrons trapped at Zn vacancy, respectively. $\lambda_B = 1/\tau_B$ is the annihilation rate at delocalized states and $\tau_B = 170$ ps the positron bulk lifetime in ZnO.[10] The positron trapping rate K_D is proportional to the defect concentration $K_D = \mu_D C_D$, where μ_D is the defect specific trapping rate per vacancy, that we have assumed to be $\mu_D = 3 \times 10^{15}$ s^{-1} at 300 K as for the Ga vacancy in GaN.[23]

Table I presents the concentration of vacancies in the films obtained from experimental data. The concentration of Zn vacancies is close to 2 ppm in films grown over the *C* and *R* planes of sapphire (without buffer layer) and also in the film grown with a buffer layer on the *R* plane. However, the film grown on the *C* plane with a buffer layer presents a large concentration of Zn vacancies (6 ppm). Interestingly, this sample presents a more intense PL emission peak at 370.5 nm (3.346 eV) than the other three samples (see Fig. 1) which have lower Zn vacancy concentration (around 2 ppm).

The concentrations of Zn vacancies in thinner samples grown over *M*, *A*, and *C* planes of sapphire are also indicated in Table I. Figure 10 shows the PL emission of *M*, *A*, and *C* samples together with the emission of samples already presented in Fig. 1 for comparison. Sample *M* with the lower Zn vacancy content shows a very low 370.5 nm PL emission, which is revealed as a slope change in the spectrum. Sample

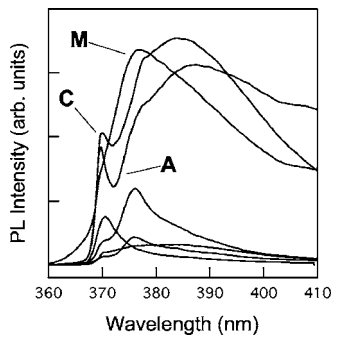

FIG. 10. Photoluminescence emission at 10 K, excited at 325 nm for samples grown over the *M*, *A*, and *C* planes of sapphire together with the emission corresponding to samples in Fig. 1.

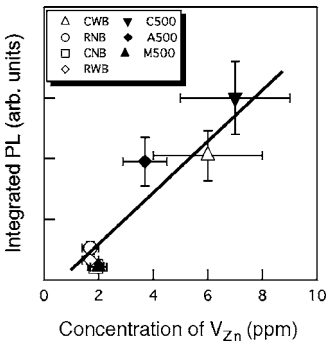

FIG. 11. Plot of the integrated area of the 370.5 nm emission against Zn vacancy concentration for the different samples. The estimated error is indicated by means of bars in both the vacancy concentration and the integrated luminescence.

A with concentrations of 3.7 ppm presents a higher 370.5 nm PL emission. In sample *C* (7 ppm) this emission becomes wider and more intense.

In order to evaluate the area of the 370.5 nm emission line we have performed a Gaussian decomposition of the PL spectra. Figure 11 presents the area of the decomposed Gaussian peak corresponding to the 370.5 nm emission line versus the Zn vacancy concentration for the different samples. Figure 11 shows the same trend for the two sets of samples (0.5 and 2 μm thick) between Zn vacancy concentration and 370.5 nm peak emission. From the results a clear relation can be inferred between the Zn vacancy concentration and 370.5 nm peak emission.

Our results indicate a relationship between the concentration of Zn vacancies and PL emission of the 370.5 nm line. Moreover, the defect involved in the PL emission has been found to be deep (ionization energy in the range of 90–125 meV). Deep recombination centers are, usually, quite complex and they, probably, are not simple vacancies. The defects responsible for the PL emission might not be single vacancies. However, as Fig. 9 indicates, its presence has a clear relation with the existence of Zn vacancies in the samples.

Munuera *et al.*[8] investigated the morphology of the thinnest films ($<$500 nm) studied in this work using scanning force microscopy. They found significant differences between morphologies depending on whether the substrate surface exhibits steps (misoriented *a*, *c*, and *r* planes) or not (*m* plane). Zubiaga *et al.*[9] found a correlation between the misorientation of the sapphire surface planes, measured by Munuera *et al.*,[8] and Zn vacancy concentration in thin films ($<$500 nm). Moreover, they also found that the Zn vacancy concentration in the films (without buffer layer) depends on their thickness and is larger close to the interface.

We have not found in the literature any hint about the origin of the 370.5 nm (3.436 eV) emission line. Meyer *et al.*[13] concluded that a sharp line of excitonic character at around 3.333 eV found in bulk ZnO shows most of the established features of *Y* recombination line commonly seen in ZnSe and ZnTe (exciton bound to dislocations and other extended structural defects). Urbieta *et al.*[24] observed in bulk ZnO samples an emission at 3.1 eV by cathodoluminescence and they concluded that it was related to dislocations.

The PL measurements presented in the present work do not allow us to state straight ahead that the 370.5 nm line corresponds to an excitonic recombination into extended structural defects. Nevertheless, Fig. 11 indicates that there is a clear correlation between the Zn vacancy concentration and the intensity of the 370.5 nm emission line. Therefore, we can assign the 370.5 nm (3.436 eV) emission to the recombination of excitons into a deep center that is related to the presence of Zn vacancies.

IV. SUMMARY

We have used photoluminescence and positron annihilation spectroscopy to study ZnO films grown by MOCVD over different planes of sapphire and characterize some of the optically active defects in the ZnO layers. Positron annihilation spectroscopy has been found very useful for the identification and quantification of vacancy-type defects in ZnO films. The found relation between the intensity of the PL spectra and Zn vacancy concentration indicates that the 370.5 nm (3.346 eV) emission line is related to the presence of Zn vacancies.

ACKNOWLEDGMENTS

This paper is dedicated to the memory of the young Professor K. Saarinen, who passed away last December. This work has been undertaken under Project Nos. MAT2004-06841 and UPV00224.310-14553/2002. One of us (A.Z.) wants to thank the Basque Government for financial support.

[1] D. C. Look, D. C. Reynolds, J. R. Sizelove, R. L. Jones, C. W. Litton, G. Cantwell, and W. Harsch, Solid State Commun. **105**, 399 (1998).
[2] Z. K. Tang, G. K. L. Wong, P. Yu, M. Kawasaki, A. Ohtomo, H. Koinuma, and Y. Segawa, Appl. Phys. Lett. **72**, 3270 (1998).
[3] D. M. Bagnall, Y. F. Chen, Z. Zhu, T. Yao, S. Koyama, M. Y. Shen, and T. Goto, Appl. Phys. Lett. **70**, 2230 (1997).
[4] D. F. Croxall, R. C. C. Ward, C. Wallace, and R. Kell, J. Cryst. Growth **22**, 117 (1974).
[5] V. Srikant and D. R. Clarke, J. Appl. Phys. **81**, 6357 (1997).
[6] Z. Q. Chen, S. Yamamoto, M. Maekawa, A. Kawasuso, X. L. Yuan, and T. Sekiguchi, J. Appl. Phys. **94**, 4807 (2003).
[7] A. Uedono, T. Koida, A. Tsukazaki, M. Kawasaki, Z. Q. Chen, S. F. Chichibu, and H. Koinuma, J. Appl. Phys. **93**, 2481 (2003).
[8] C. Munuera, J. Zúñiga Pérez, J. F. Rommeluere, V. Sallet, R. Triboulet, F. Soria, V. Múñoz-Sanjosé, and C. Ocal, J. Cryst. Growth **264**, 70 (2004).
[9] A. Zubiaga, F. Tuomisto, F. Plazaola, K. Saarinen, J. A. García, J. F. Rommeluere, J. Zúñiga Pérez, and V. Múñoz-Sanjosé, Appl. Phys. Lett. **86**, 042103 (2005).
[10] F. Tuomisto, V. Ranki, K. Saarinen, and D. Look, Phys. Rev. Lett. **91**, 205502 (2003).
[11] D. Bimberg, M. Sondergeld, and E. Grobe, Phys. Rev. B **4**, 3451 (1971).
[12] D. W. Hamby, D. A. Lucca, J. Kolpfstein, and G. Cantwell, J. Appl. Phys. **93**, 3214 (2003).
[13] B. K. Meyer *et al.*, Phys. Status Solidi B **241**, 231 (2004).
[14] Y. P. Varshni, Physica (Amsterdam) **34**, 147 (1967).
[15] M. O. Manasreh, Phys. Rev. B **53**, 16425 (1996).
[16] E. Kaldis, *Current Topics in Materials Science* (North-Holland, Amsterdam, 1982), Vol. 9.
[17] S. C. Abrahams and J. L. Berstein, Acta Crystallogr., Sect. B: Struct. Crystallogr. Cryst. Chem. **25**, 1233 (1969).
[18] A. R. Hutson, J. Phys. Chem. Solids **8**, 467 (1959).
[19] J. R. Haynes, Phys. Rev. Lett. **4**, 361 (1960).
[20] J. Gutowski, N. Presser, and I. Broser, Phys. Rev. B **38**, 9746 (1988).

[21]S. A. Studenikin, M. Cocivera, W. Kellner, and H. Pascher, J. Lumin. **91**, 23 (2000).
[22]K. Saarinen, P. Hautojarvi, and C. Corbel, *Identification of Defects in Semiconductors* (Academic, New York, 1998).
[23]K. Saarinen, T. Suski, I. Grzegory, and D. C. Look, Phys. Rev. B **64**, 233201 (2001).
[24]A. Urbieta, P. Fernández, J. Piqueras, C. Hardalov, and T. Sekiguchi, J. Phys. D **34**, 2945 (2001).